# Cooperative Nano Communication in the THz Gap Frequency Range using Wireless Power Transfer

**A. Chaminda J. Samarasekera[1] and Hyundong Shin[2*]**
[1]Kyung Hee University
Youngin 446-701 - Korea
[e-mail: samarasekera@khu.ac.kr]
[2] Kyung Hee University
Youngin 446-701 - Korea
[e-mail: hshin@khu.ac.kr]
*Corresponding author: Hyundong Shin

*Received May 4, 2017; revised February 22, 2018; revised May 14, 2018; revised September 28, 2018; accepted April 18, 2019; published October 31, 2019*

## Abstract

Advancements in nanotechnology and novel nano materials in the past decade have provided a set of tools that can be used to design and manufacture integrated nano devices, which are capable of performing sensing, computing, data storing and actuation. In this paper, we have proposed cooperative nano communication using Power Switching Relay (PSR) Wireless Power Transfer (WPT) protocol and Time Switching Relay (TSR) WPT protocol over independent identically distributed (i.i.d.) Rayleigh fading channels in the Terahertz (THz) Gap frequency band to increase the range of transmission. Outage Probability (OP) performances for the proposed cooperative nano communication networks have been evaluated for the following scenarios: A) A single decode-and-forward (DF) relay for PSR protocol and TSR protocol, B) DF multi-relay network with best relay selection (BRS) for PSR protocol and TSR protocol, and C) DF multi-relay network with multiple DF hops with BRS for PSR protocol and TSR protocol. The results have shown that the transmission distance can be improved significantly by employing DF relays with WPT. They have also shown that by increasing the number of hops in a relay the OP performance is only marginally degraded. The analytical results have been verified by Monte-Carlo simulations.

***Keywords:*** Terahertz Band, Nanonetworks, Channel Model, Cooperative Communication, Outage Probability, Wireless Power Transfer.

**http://doi.org/10.3837/tiis.2019.10.012** **ISSN : 1976-7277**

## 1. Introduction

The advancements made in nanotechnology and novel nano materials in the past decade have made it possible for many innovative applications in different fields such as biomedical, environmental, military, etc. to be developed. Nanotechnology has enabled devices to be built in the range of 1 to a few hundred nanometers which are capable of performing basic tasks as sensing, relaying, etc. as discussed in [1] and [2].

Richard Feynman first envisioned nanotechnology in 1959 in a speech titled "There's Plenty of Room at the Bottom". Nanotechnology have enabled engineers to design and manufacture integrated devices which are capable of performing many basic applications, but also more complex functions with communication, control and coordination among the nano machines [3]. A new type of wireless sensor network has been developed by combining nanotechnology and materials science theory, called bionanosensor networks in [4]. These bionanosensor networks are composed of a number of nanomachines with the ability to sense chemical signals. Nano sensors are actually nano machines that are capable of taking advantage of properties of novel nanomaterials, such as Graphene that can detect chemical compounds as low as one part per billion, presence of viruses and bacteria [5].

Graphene, a single layer of carbon packed in a hexagonal lattice with a carbon-carbon distance of 0.142nm, is the first truly two-dimensional crystalline material, and is representative of a whole class of 2D materials. Graphene is extremely thin, mechanically very strong, flexible, transparent, and is a conductor. These properties make it interesting for applications in flexible electronics, gas sensing, and due to its low weight, for many applications in aircrafts, satellites, and others [6]. Graphene Nanoribbons and Carbon Nanotubes have enabled the development of nano-batteries, nano-memories, nano-sensors, and nano-actuators, which take advantage of the unique properties observed in nanomaterials and its derivatives [7]. In [8], [9], and [10], THz frequency band nano antennas made of Graphene have been proposed and their performances have been investigated.

In the electromagnetic spectrum located between the millimeter waves and infrared light waves are the THz waves, which have been rarely utilized except for astronomy and fields related to astronomy [11]. In [12] and [13], THz waves in the range of 0.1 THz - 10 THz for future wireless communication and technologies have been investigated. A review of the applications related to THz wave technologies and communications are discussed by Ho-Jin Song and Nagatsuma in [14]. The total path loss of a propagating wave in the terahertz band depends on the frequency, distance and the composition of the transmission medium at a molecular level [5]. Furthermore, in [5], a channel model for electromagnetic wireless nanonetworks in the terahertz band has been introduced, and the capacity of the nanonetwork has been analyzed.

One of the hurdles for nano machines has been the amount of power that the nano machines are capable of producing, which has been around 800pJ so far [15], [16], [17], and [18]. However, by incorporating WPT techniques, it is possible to provide the necessary power that nano machines require for wireless data transmission. Nikola Tesla described the freedom to transfer energy between two points without the need for a physical connection to a power source as an “all-surpassing importance to man” [19] and [20]. Power transmission by radio waves dates back to the early work of Heinrich Hertz [21], where he demonstrated electromagnetic wave propagation in free space using a complete system with a spark gap to generate high-frequency power and to detect it at the receiving end. Power transmission is a three-step process where 1) dc electrical power is converted to RF power, 2) the RF power is then transmitted through free space to the receiver, and 3) the power is collected and

converted back into dc power at the receiving point, [21]. In practice, WPT is usually implemented based on one of these three different technologies: 1) inductive coupling [22], 2) magnetic resonance coupling [23], or 3) microwave power transfer [21], respectively for short range (centimeter range), mid range (several meter range), and long range (up to tens of kilometer range), [24]. In [25], Varshney first proposed transmitting information and energy simultaneously. A time switching receiver (TSR) protocol and a power switching receiver (PSR) protocal are proposed in [26]. A practical point-to-point wireless simultaneous information and power transfer scheme is proposed, and the concept is further extended to multiple-input multiple-output (MIMO) systems in [27]. Energy harvesting is an effective and efficient means to prolong the life of wireless networks and increase the range of transmission with increase of power. In [28], a best cooperation mechanism for cooperative 5G network that can harvest energy and transmit data simulteneously in timeslot mode has been proposed.

We have proposed in this paper using cooperative communication techniques with wireless power transfer to increase the transmission range of nano machines in the THz Gap frequency range for non-line-of-sight communication. By making advances in wireless nanosensor networks, it is possible to enable health monitoring, surveillance of weapons of mass destruction, etc [5].

The rest of this paper has been organized as follows: in Section II, THz wave propagation, wireless power transfer and relay models are explained; in Section III, outage probability has been calculated for: A) A single DF relay for PSR protocol and TSR protocol, B) multiple DF relays with BRS for PSR protocol and TSR protocol, and C) multiple DF relays with multiple DF hops with BRS for PSR protocol, and TSR protocol; in Section IV, the numerical calculations are validated by simulations, and the results are investigated; finally, the paper is summarized and conclusions are presented in Section V.

## 2. Propagation, Wireless Power Transfer and Relaying Models

### 2.1 Terahertz Propagation Model

A propagation model for Graphene-based nano-tranceivers in the Terahertz band (0.1 - 10.0 THz) is given in [5], where path loss and noise power have been calculated as follows

#### 2.1.1 Path loss

The total path loss for an electromagnetic wave in the Terahertz band can be written as follows

$$A(f,d) = A_{spread}(f,d) + A_{absorption}(f,d), \#(1)$$

where $A_{spread}(f,d)$ denotes the spreading loss of the signal and $A_{absorption}(f,d)$ denotes the signal attenuation due to molecular absorption. The spreading loss can be written as

$$A_{spread}(f,d) = 20log\left(\frac{4\pi fd}{c}\right), \#(2)$$

and the molecular absorption attenuation can be written as

$$A_{absorption} = \frac{1}{\tau(f,d)} = e^{k(f)d}. \#(3)$$

Transmittance of medium, $\tau$ , has been obtained using the Beer-Lambert Law as

$$\tau(f,d) = \frac{P_0}{P_i} = e^{-k(f)d}, \#(4)$$

where $f$ is the frequency of the electromagnetic wave considered, $d$ is the total path length, $P_0$ and $P_i$ are the radiated and incident powers, and $k$ is the medium absorption coefficient. The absorption coefficient for the composition of molecules found along the path can be defined as

$$k(f) = \sum_{i,g} k^{i,g}(f) \ , \#(5)$$

where absorption coefficient of the isotopologue $i$ of gas $g$ is $k^{i,g}$ in $m^{-1}$ and is calculated as

$$k^{i,g}(f) = \frac{p}{p_0}\frac{T_{stp}}{T} Q^{i,g}\sigma^{i,g}(f). \#(6)$$

$Q^{i,g}$, $p$, $T$, $p_0$, $T_{stp}$ and $\sigma^{i,g}$ are respectively the volumetric density in $molecules/m^3$, pressure, temperature, standard pressure, standard temperature, and the absorption cross section for the isotopologue $i$ of gas $g$ in $m^2/molecule$. The total number of molecules per unit volume, $Q^{i,g}$, of the isotopologue $i$ of gas $g$ for the given gas mixture can be calculated using the Ideal Gas Law as

$$Q^{i,g} = \frac{p}{RT} q^{i,g} N_A, \#(7)$$

where $R$ is the gas constant, $q^{i,g}$ is the mixing ratio for the isotopoloque $i$ of gas $g$, and $N_A$ stand for the Avogadro constant. $\sigma^{i,g}$ can be defined as

$$\sigma^{i,g} = S^{i,g} G^{i,g}(f), \#(8)$$

where $S^{i,g}$ is the line intensity which can be directly obtained from the High Resolution Transmission (HITRAN) database. $S^{i,g}$ defines the strength of the absorption by a specific type of molecules. $G^{i,g}$ is the line shape; the continuum absorption at the far ends of the line shape can be accounted as proposed in [29] and subsequently used in [5] as

$$G^{i,g}(f) = \frac{f}{f_c^{i,g}} \frac{tanh\left(\frac{hcf}{2k_BT}\right)}{tanh\left(\frac{hcf_c^{i,g}}{2k_BT}\right)} F^{i,g}(f), \#(9)$$

where $h$ is the Planck constant, $c$ is the speed of light in a vacuum, $k_B$ is the Boltzmann constant, and $T$ is the system temperature. To obtain the line shape, $G^{i,g}$, the resonant frequency $f_c^{i,g}$ for the isotopologue $i$ of gas $g$ has to be determined as follows

$$f_c^{i,g} = f_{c0}^{i,g} + \delta^{i,g}\frac{p}{p_0}, \#(10)$$

where $f_{c0}^{i,g}$ is the zero-pressure position of the resonance, and $\delta^{i,g}$ is the linear pressure shift. These parameters can be directly obtained from the HITRAN database. Van Vleck-Wisskopf asymmetric line shape [30] has been considered for the representation of molecular absorption

$$F^{i,g}(f) = 100c\frac{\alpha_L^{i,g}}{\pi}\frac{f}{f_c^{i,g}}\left[\frac{1}{\left(f - f_c^{i,g}\right)^2 + \left(\alpha_L^{i,g}\right)^2} + \frac{1}{\left(f + f_c^{i,g}\right)^2 + \left(\alpha_L^{i,g}\right)^2}\right], \#(11)$$

where $f$, $c$, $\alpha_L^{i,g}$, and $f_c^{i,g}$ are respectively the frequency considered, speed of light in a vacuum, Lorentz half-width coefficient for isotopologue $i$ of gas $g$, and resonant frequency for the isotopologue $i$ of gas $g$. Lorentz half-width can be obtained as a function of air-broadened half-width $\alpha_0^{air}$ and self-broadened half-width $\alpha_0^{i,g}$ as follows

$$\alpha_L^{i,g} = \left[(1 - q^{i,g})\alpha_0^{i,g} + q^{i,g}\alpha_0^{i,g}\right]\left(\frac{p}{p_0}\right)\left(\frac{T_0}{T}\right)^{\gamma}, \#(12)$$

where $q^{i,g}$, $p$, $p_0$, $T_0$, $T$, and $\gamma$ are respectively the mixing ratio for the isotopologue $i$ of gas $g$, system pressure, reference pressure, reference temperature, system temperature, and temperature broadening coefficient. The values for $\gamma$, $\alpha_0^{air}$, and $\alpha_0^{i,g}$ can be directly obtained from the HITRAN database.

### 2.1.2 Noise Power

The total noise of the system contains molecular absorption noise, antenna noise temperature, system noise temperature, etc.

$$T_{noise} = T_{system} + T_{molecular} + T_{other}. \#(13)$$

The noise power at the receiver can be calculated as follows for a given bandwidth

$$P_n(f,d) = \int_B N(f,d)\,df = k_B \int_B T_{noise}(f,d)\,df, \#(14)$$

where $f$, $d$, $N$, $k_B$, and $T_{noise}$ are respectively the frequency considered, transmission distance, noise power spectral density, Boltzmann constant, and equivalent noise temperature. The molecular absorption noise introduced during the propagation of the electromagnetic waves in the terahertz band can be calculated as follows. The parameter that measures this phenomenon is known as the emissivity of the channel, $\varepsilon$

$$\varepsilon(f,d) = 1 - \tau(f,d), \#(15)$$

where $\tau$ is the transmissivity of the medium given from equation (4) [5]. The noise temperature due to molecular absorption $T_{molecular}$ that an omnidirectional antenna detects from the medium can be obtained as follows in Kelvin

$$T_{molecular}(f,d) = T_0\varepsilon(f,d), \#(16)$$

$T_0$ and $\varepsilon$ are respectively the reference temperature and emissivity of the channel [5]. It is assumed for this paper that graphene based electronics devices are very low noise, and therefore, only molecular noise absorption is considered.

## 2.2 Wireless Power Transfer

Energy harvesting is an effective means to prolong the life and range of a wireless network. A simultaneous wireless information and power transfer scheme is proposed in [31] and [25]. The harvested energy stored in the battery, denoted by $Q$ in joule, is given by

$$Q = \zeta\mathbb{E}[i_{DC}(t)] = \zeta hP, \#(17)$$

where $\zeta$ is the conversion efficiency $0 < \zeta < 1$ and P is the received signal power. Two practically realizable receiver designs have been proposed in [32], namely time-switching receivers and power-switching receivers.

### 2.2.1 Time Switching-Based Relaying Protocol

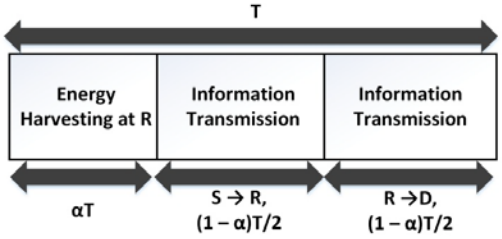


**Fig. 1.** TSR protocol

For the TSR Protocol in **Fig. 1**, $T$ is the block of time during which information and power

are transmitted; $\alpha$ is the fraction of time that is used for harvesting energy, and the remaining time $(1-\alpha)T$ is used for information transmission, where $\alpha$ is $0 < \alpha < 1$. All the energy harvested during the harvesting phase is consumed during the transmission of the information. The harvested energy can be written as follows from [32]

$$E_h = \frac{\eta P_b |h|^2}{A_i} \alpha T, \#(18)$$

where $\eta$ is the energy conversion efficiency, $0 < \eta < 1$, which depends on rectification process and energy harvesting circuitry, $h$ denotes the channel coefficient of the wireless power transmission link, $P_b$ is the transmitted power from the power beacon [33], and $A_i$ represents the total pathloss of the electromagnetic wave transmission.

### 2.2.2 Power Switching-Based Relaying Protocol

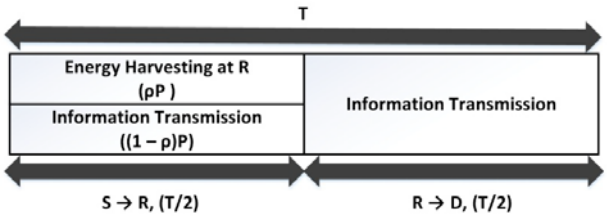


**Fig. 2.** PSR protocol

From **Fig. 2**, it is possible to see that $T$ is the total block time at the node. During the first half of the block, $\rho P_b$ is used for energy harvesting, and $(1-\rho)P_b$ is used for information transmission. $\rho$ is the choice of power fraction used at the node for energy harvesting where $\rho$ is $0 < \rho < 1$. It is assumed that all the harvested energy is consumed during the information transmission. The harvested energy at the node can be given as follows from [32]

$$E_h = \frac{\eta \rho P_b |h|^2}{A_i} \left(T/2\right), \#(19)$$

where $\eta$ is the energy conversion efficiency, $0 < \eta < 1$, which depends on rectification process and energy harvesting circuitry, $h$ denotes the channel coefficient of the wireless power transmission link, $P_b$ is the transmitted power from the power beacon [33], and $A_i$ represents the total pathloss of the electromagnetic wave transmission.

## 2.3 Relay Models

In this paper, decode-and-forward relaying scheme has been employed at all relays and hops. Where there are multiple relays, BRS scheme has been employed, and PSR protocol and TSR protocol have been used for WPT to increase the range of transmission over Rayleigh fading channels. $P_{PB}$ represents the transmitted signal power from the power beacon, $A_i$ represents the total pathloss of the electromagnetic wave in the Terahertz band due to molecular absorption attenuation and spreading loss, and $N_i$ is the total noise.

### 2.3.1 Single DF Relay

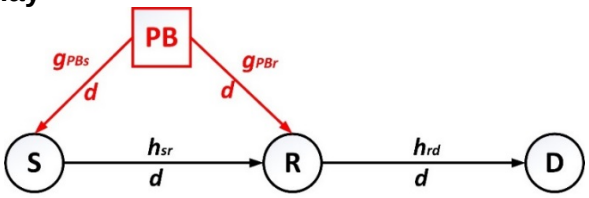


**Fig. 3.** Single DF Relay using WPT

A cooperative nano relaying network as in **Fig. 3**, where data is transmitted from the source nano machine to the destination nano machine through a relaying nano machine, has been considered. $h_{sr}$ denotes the channel coefficient of the Source to Relay link, $h_{rd}$ denotes the channel coefficient of the Relay to Destination link, $g_{PB_S}$ denotes the channel coefficient of the Power Beacon to Source link, and $g_{PB_R}$ denotes the channel coefficient of the Power Beacon to Relay link. The instantaneous end-to-end signal-to-noise ratio (SNR) can be written as

$$\gamma_d = \min\left( \alpha_{sr}|h_{sr}|^2\left|g_{PB_S}\right|^2, \alpha_{rd}|h_{rd}|^2\left|g_{PB_R}\right|^2\right), \#(20)$$

where for TSR Protocol $\alpha_i = \frac{2\eta\alpha P_{PB}}{A_i A_{PB_i}(1-\alpha)N_i}$, and for PSR Protocol $\alpha_i = \frac{\eta\rho(1-\rho)P_{PB}}{A_i A_{PB_i} N_i}$. $\gamma_{sr} = \alpha_{sr}|h_{sr}|^2\left|g_{PB_S}\right|^2$ represents Source to Relay SNR, and $\gamma_{rd} = \alpha_{rd}|h_{rd}|^2\left|g_{PB_R}\right|^2$ represents Relay to Destination SNR. Furthermore, $\gamma_d$ represents the end-to-end SNR for $S \rightarrow R \rightarrow D$.

### 2.3.2 Multiple DF Relays with BRS

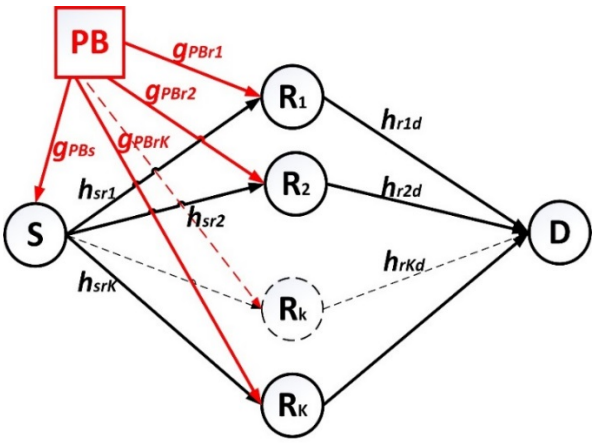


**Fig. 4.** Multiple DF Relays with BRS using WPT

A cooperative nano relaying network as in **Fig. 4** has been considered. The data is transmitted from the source nano machine to the destination nano machine through multiple relaying nano machines, where the best relay is selected for information transmission. $h_{sr_k}$ denotes the channel coefficient of the link$S \rightarrow R_k$, $h_{r_k d}$ denotes the channel coefficient of the link $R_k \rightarrow D$, $g_{PB_s}$ denotes the channel coefficient of the link $PB \rightarrow S$, and $g_{PB_{R_k}}$ denotes the channel coefficient of the link $PB_{R_k} \rightarrow R_k$. The end-to-end SNR can be written as

$$\gamma_d = \max_{k = 1,2,\ldots,K} (\gamma_k), \#(21)$$

and $\gamma_k$ can be determined by

$$\gamma_k = \min_{k = 1,2,\ldots,K}\left( \alpha_{sr_k}\left|h_{sr_k}\right|^2\left|g_{PB_S}\right|^2, \alpha_{r_k d}\left|h_{r_k d}\right|^2\left|g_{PB_{R_k}}\right|^2\right), \#(22)$$

where for TSR Protocol $\alpha_i = \frac{2\eta\alpha P_{PB}}{A_i A_{PB_i}(1-\alpha)N_i}$, and for PSR Protocol $\alpha_i = \frac{\eta\rho(1-\rho)P_{PB}}{A_i A_{PB_i} N_i}$. $\gamma_{sr_k} = \alpha_{sr_k}\left|h_{sr_k}\right|^2\left|g_{PB_S}\right|^2$ represents $S \rightarrow R_k$ SNR, and $\gamma_{r_k d} =$

$\alpha_{r_k d}\left|h_{r_k d}\right|^2\left|g_{PB_{R_k}}\right|^2$ represents $R_k \rightarrow D$ SNR. $\gamma_k$ represents the SNR for each particular relay. Furthermore, $\gamma_d$ represents the end-to-end SNR for $S \rightarrow R_k \rightarrow D$.

### 2.3.3 Multiple DF Relays with Multiple DF Hops using BRS

A cooperative nano relaying network as in **Fig. 5**, where the data is transmitted from the source nano machine to the destination nano machine through relaying nano machines, has been considered. $h_{sr_{1k}}$ denotes the channel coefficient of the link $S \rightarrow R_{1k}$, $h_{r_{Nk}d}$ denotes the channel coefficient of the link $R_{Nk} \rightarrow D$, $g_{PB_s}$ denotes the channel coefficient of the link $PB \rightarrow S$, and $g_{PB_{Nk}}$ denotes the channel coefficient of the link $PB \rightarrow R_{n,k}$.

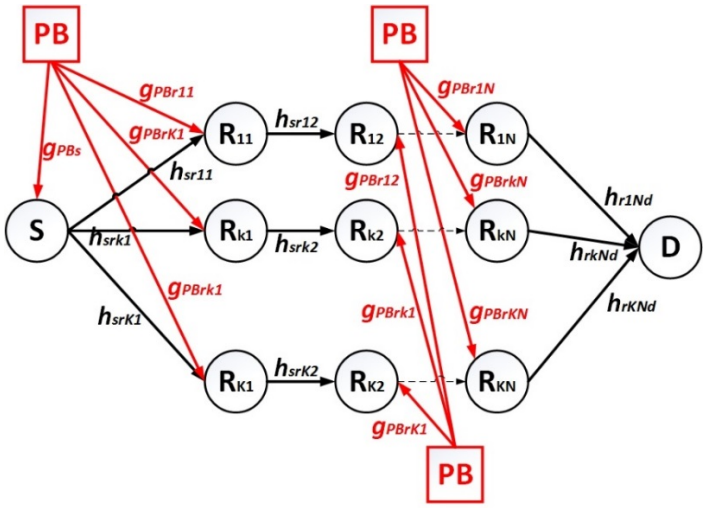


**Fig. 5.** Multiple DF Relays with Multiple DF Hops with BRS using WPT

The end-to-end SNR can be written as

$$\gamma_d = \max_{k = 1,2,\ldots,K} (\gamma_k), \#(23)$$

and $\gamma_k$ can be determined by

$$\gamma_k = \min_{k = 1,2,\ldots,K} \left( \alpha_{sr_{1k}}\left|h_{sr_{1k}}\right|^2\left|g_{PB_S}\right|^2, \ldots, \alpha_{r_{Nk}d}\left|h_{r_{Nk}d}\right|^2\left|g_{PB_{R_{Nk}}}\right|^2 \right), \#(24)$$

where for TSR Protocol $\alpha_i = \frac{2\eta\alpha P_{PB}}{A_i A_{PB_i}(1-\alpha)N_i}$, and for PSR Protocol $\alpha_i = \frac{\eta\rho(1-\rho)P_{PB}}{A_i A_{PB_i} N_i}$. $\gamma_{1k} = \alpha_{sr_{1k}}\left|h_{sr_{1k}}\right|^2\left|g_{PB_S}\right|^2$ represents $S \rightarrow R_{1k}$ SNR, and $\gamma_{Nk} = \alpha_{sr_{Nk}}\left|h_{sr_{Nk}}\right|^2\left|g_{PB_{R_{Nk}}}\right|^2$ represents $R_{Nk} \rightarrow D$ SNR. Furthermore, $\gamma_d$ represents the end-to-end SNR for $S \rightarrow R_{Nk} \rightarrow D$.

## 3. Outage Probability

Outage probability is the probability that the instantaneous SNR at the receiver falls below a threshold SNR $\gamma_{th}$. $P_{PB}$ is the transmitted power from the power beacon, $A_i(f,d)$ is the total pathloss of the electromagnetic wave in the Terahertz band due to molecular absorption attenuation and spreading loss, $N_i(f,d)$ is the noise power, $\eta$ is the energy conversion efficiency, $\alpha$ is the fraction of time that is used for harvesting energy, and $\rho$ is the choice of

power fraction used at the node for energy harvesting. $\sigma_{y_1}$, $\sigma_{y_2}$ , $\sigma_{x_1}$, and $\sigma_{x_2}$ are the Rayleigh channel fading parameters. Function $K_\upsilon(z)$ is as explained in [34].

### 3.1 Single DF Relay

The OP for a single DF Relay using WPT, as in **Fig. 3**, can be calculated as follows. Since $\gamma_{sr}$ and $\gamma_{rd}$ are independent Rayleigh distributed random variables, the cumulative distributive functions (CDFs) for $\gamma_{sr}$ and $\gamma_{rd}$ can be written as

$$F_{\gamma_{sr}}(\gamma_{th}) = \int_0^\infty F_{y_1}\left(\frac{\gamma_{th}}{\alpha_{sr}x_1}\right) f_{x_1}(x_1)dx_1 \,, \#(25)$$

$$F_{\gamma_{rd}}(\gamma_{th}) = \int_0^\infty F_{y_2}\left(\frac{\gamma_{th}}{\alpha_{rd}x_2}\right) f_{x_2}(x_2)dx_2 \,, \#(26)$$

where $y_1 = |h_{sr}|^2$, $y_2 = |h_{rd}|^2$, $x_1 = \left|g_{PB_S}\right|^2$, and $x_2 = \left|g_{PB_R}\right|^2$. After some mathematical manipulations (25) and (26) can be written as

$$F_{\gamma_{sr}}(\gamma_{th}) = \int_0^\infty \frac{x_1}{\sigma_{x_1}^2} e^{-x_1^2/2\sigma_{x_1}^2} dx_1 - \int_0^\infty \frac{x_1}{\sigma_{x_1}^2} e^{-x_1^2/2\sigma_{x_1}^2} e^{-\left(\frac{\gamma_{th}}{\alpha_{sr}x_1}\right)^2/2\sigma_{y_1}^2} dx_1 \,, \#(27)$$

$$F_{\gamma_{rd}}(\gamma_{th}) = \int_0^\infty \frac{x_2}{\sigma_{x_2}^2} e^{-x_2^2/2\sigma_{x_2}^2} dx_2 - \int_0^\infty \frac{x_2}{\sigma_{x_2}^2} e^{-x_2^2/2\sigma_{x_2}^2} e^{-\left(\frac{\gamma_{th}}{\alpha_{rd}x_2}\right)^2/2\sigma_{y_2}^2} dx_2 \,. \#(28)$$

(27) and (28) can be calculated using [ [34], page 337, Eq. 3.326, $2^{10}$] and [ [34], page 370, Eq. 3.478, 4], and can be written as

$$F_{\gamma_{sr}}(\gamma_{th}) = \Gamma(1) - \frac{\gamma_{th}}{\alpha_{sr}\sigma_{x_1}\sigma_{y_1}} K_1\left(\frac{\gamma_{th}}{\alpha_{sr}\sigma_{x_1}\sigma_{y_1}}\right), \#(29)$$

$$F_{\gamma_{rd}}(\gamma_{th}) = \Gamma(1) - \frac{\gamma_{th}}{\alpha_{rd}\sigma_{x_2}\sigma_{y_2}} K_1\left(\frac{\gamma_{th}}{\alpha_{rd}\sigma_{x_2}\sigma_{y_2}}\right). \#(30)$$

The end-to-end CDF of $\gamma_d$ of the relay can be calculated as

$$F_{\gamma_d}(\gamma_{th}) = \left[1 - \left(1 - F_{\gamma_{sr}}(\gamma_{th})\right)\left(1 - F_{\gamma_{rd}}(\gamma_{th})\right)\right]. \#(31)$$

After substituting (29), (30) in (31), $F_{\gamma_d}(\gamma_{th})$ can be written as

$$F_{\gamma_d}(\gamma_{th}) = 1 - \frac{\gamma_{th}^2}{\alpha_{sr}\alpha_{rd}\sigma_{x_1}\sigma_{y_1}\sigma_{x_2}\sigma_{y_2}} K_1\left(\frac{\gamma_{th}}{\alpha_{sr}\sigma_{x_1}\sigma_{y_1}}\right) K_1\left(\frac{\gamma_{th}}{\alpha_{rd}\sigma_{x_2}\sigma_{y_2}}\right). \#(32)$$

#### 3.1.1 OP for TSR protocol

The OP for single DF relay using WPT protocol TSR can be written as follows by substituting the values for $\alpha_{sr} = \frac{2\eta\alpha P_{PB}}{A_{sr}A_{PB_S}(1-\alpha)N_{sr}}$ and $\alpha_{rd} = \frac{2\eta\alpha P_{PB}}{A_{rd}A_{PB_R}(1-\alpha)N_{rd}}$ in (32).

$$P_{Out}(f,d) = 1 - \frac{\gamma_{th}^2 A_{sr}A_{PB_S}A_{rd}A_{PB_R}(1-\alpha)^2 N_{sr}N_{rd}}{4\eta^2\alpha^2(P_{PB})^2\sigma_{x_1}\sigma_{y_1}\sigma_{x_2}\sigma_{y_2}} \#(33)$$

$$\times K_1\left(\frac{\gamma_{th}A_{sr}A_{PB_S}(1-\alpha)N_{sr}}{2\eta\alpha P_{PB}\sigma_{x_1}\sigma_{y_1}}\right) K_1\left(\frac{\gamma_{th}A_{rd}A_{PB_R}(1-\alpha)N_{rd}}{2\eta\alpha P_{PB}\sigma_{x_2}\sigma_{y_2}}\right).$$

### 3.1.2 OP for PSR Protocol

The OP for single DF relay using WPT protocol PSR can be written as follows by substituting the values for $\alpha_{sr} = \frac{\eta\rho(1-\rho)P_{PB}}{A_{sr}A_{PB_S}N_{sr}}$ and $\alpha_{rd} = \frac{\eta\rho(1-\rho)P_{PB}}{A_{rd}A_{PB_R}N_{rd}}$ in (32).

$$P_{Out}(f,d) = 1 - \frac{\gamma_{th}^2 A_{sr}A_{PB_S}A_{rd}A_{PB_R}N_{sr}N_{rd}}{\eta^2\rho^2(1-\rho)^2(P_{PB})^2\sigma_{x_1}\sigma_{y_1}\sigma_{x_2}\sigma_{y_2}} \#(34)$$
$$\times K_1\left(\frac{\gamma_{th}A_{sr}A_{PB_S}N_{sr}}{\eta\rho(1-\rho)P_{PB}\sigma_{x_1}\sigma_{y_1}}\right)K_1\left(\frac{\gamma_{th}A_{rd}A_{PB_R}N_{rd}}{\eta\rho(1-\rho)P_{PB}\sigma_{x_2}\sigma_{y_2}}\right).$$

### 3.2 Multiple DF Relays with BRS

The OP for multiple DF relays with BRS using WPT, as in **Fig. 4**, can be calculated as in [35], [36]

$$F_{\gamma_d}(\gamma_{th}) = \prod_{k=1}^{K} F_{\gamma_k}(\gamma_{th}), \#(35)$$

where $F_{\gamma_k}(\gamma_{th})$ can be express as

$$F_{\gamma_k}(\gamma_{th}) = \left[1 - \left(1 - F_{\gamma_{sr_k}}(\gamma_{th})\right)\left(1 - F_{\gamma_{r_kd}}(\gamma_{th})\right)\right]. \#(36)$$

Since $\gamma_{sr_k}$ and $\gamma_{r_kd}$ are independent Rayleigh distributed random variables, the CDFs of $F_{\gamma_{sr_k}}(\gamma_{th})$ and $F_{\gamma_{r_kd}}(\gamma_{th})$ can be written as

$$F_{\gamma_{sr_k}}(\gamma_{th}) = \int_0^\infty F_{y_1}\left(\frac{\gamma_{th}}{\alpha_{sr_k}x_1}\right)f_{x_1}(x_1)dx_1, \#(37)$$

$$F_{\gamma_{r_kd}}(\gamma_{th}) = \int_0^\infty F_{y_2}\left(\frac{\gamma_{th}}{\alpha_{r_kd}x_2}\right)f_{x_2}(x_2)dx_2. \#(38)$$

where $y_1 = |h_{sr_k}|^2$, $y_2 = |h_{r_kd}|^2$, $x_1 = |g_{PB_s}|^2$, and $x_2 = |g_{PB_{R_k}}|^2$. After some mathematical manipulations (37) and (38) can be written as

$$F_{\gamma_{sr_k}}(\gamma_{th}) = \int_0^\infty \frac{x_1}{\sigma_{x_1}^2} e^{-x_1^2/2\sigma_{x_1}^2} dx_1 - \int_0^\infty \frac{x_1}{\sigma_{x_1}^2} e^{-x_1^2/2\sigma_{x_1}^2} e^{-\left(\frac{\gamma_{th}}{\alpha_{sr_k}x_1}\right)^2/2\sigma_{y_1}^2} dx_1, \#(39)$$

$$F_{\gamma_{r_kd}}(\gamma_{th}) = \int_0^\infty \frac{x_2}{\sigma_{x_2}^2} e^{-x_2^2/2\sigma_{x_2}^2} dx_2 - \int_0^\infty \frac{x_2}{\sigma_{x_2}^2} e^{-x_2^2/2\sigma_{x_2}^2} e^{-\left(\frac{\gamma_{th}}{\alpha_{r_kd}x_2}\right)^2/2\sigma_{y_2}^2} dx_2. \#(40)$$

(39) and (40) can be calculated using [ [34], page 337, Eq. 3.326, $2^{10}$] and [ [34], page 370, Eq. 3.478, 4], and can be written as

$$F_{\gamma_{sr_k}}(\gamma_{th}) = \Gamma(1) - \frac{\gamma_{th}}{\alpha_{sr_k}\sigma_{x_1}\sigma_{y_1}} K_1\left(\frac{\gamma_{th}}{\alpha_{sr_k}\sigma_{x_1}\sigma_{y_1}}\right), \#(41)$$

$$F_{\gamma_{r_kd}}(\gamma_{th}) = \Gamma(1) - \frac{\gamma_{th}}{\alpha_{r_kd}\sigma_{x_2}\sigma_{y_2}} K_1\left(\frac{\gamma_{th}}{\alpha_{r_kd}\sigma_{x_2}\sigma_{y_2}}\right). \#(42)$$

By substituting (41), (42) in (36) it is possible to write $F_{\gamma_k}(\gamma_{th})$ as

$$F_{\gamma_k}(\gamma_{th}) = 1 - \frac{\gamma_{th}^2}{\alpha_{sr_k}\alpha_{r_kd}\sigma_{x_1}\sigma_{y_1}\sigma_{x_2}\sigma_{y_2}} K_1\left(\frac{\gamma_{th}}{\alpha_{sr_k}\sigma_{x_1}\sigma_{y_1}}\right) K_1\left(\frac{\gamma_{th}}{\alpha_{r_kd}\sigma_{x_2}\sigma_{y_2}}\right), \#(43)$$

by substituting (43) in (35), it can be stated as follows

$$F_{\gamma_d}(\gamma_{th}) = \prod_{k=1}^{K} 1 - \frac{\gamma_{th}^2}{\alpha_{sr_k}\alpha_{r_kd}\sigma_{x_1}\sigma_{y_1}\sigma_{x_2}\sigma_{y_2}} K_1\left(\frac{\gamma_{th}}{\alpha_{sr_k}\sigma_{x_1}\sigma_{y_1}}\right) K_1\left(\frac{\gamma_{th}}{\alpha_{r_kd}\sigma_{x_2}\sigma_{y_2}}\right). \#(44)$$

For i.i.d. Rayleigh fading channels, it is possible to further simplify (44) to

$$F_{\gamma_d}(\gamma_{th}) = \left[1 - \frac{\gamma_{th}^2}{\alpha_{sr_k}\alpha_{r_kd}\sigma_{x_1}\sigma_{y_1}\sigma_{x_2}\sigma_{y_2}} K_1\left(\frac{\gamma_{th}}{\alpha_{sr_k}\sigma_{x_1}\sigma_{y_1}}\right) K_1\left(\frac{\gamma_{th}}{\alpha_{r_kd}\sigma_{x_2}\sigma_{y_2}}\right)\right]^K. \#(45)$$

Applying the following mathematical identity

$$(1+x)^n = \sum_{k=0}^{n} \binom{n}{k} x^k, \#(46)$$

to (45), it can be written as

$$F_{\gamma_d}(\gamma_{th}) = \sum_{j=0}^{K} \binom{K}{j} (-1)^j \left[\frac{\gamma_{th}^2}{\alpha_{sr_k}\alpha_{r_kd}\sigma_{x_1}\sigma_{y_1}\sigma_{x_2}\sigma_{y_2}} K_1\left(\frac{\gamma_{th}}{\alpha_{sr_k}\sigma_{x_1}\sigma_{y_1}}\right) K_1\left(\frac{\gamma_{th}}{\alpha_{r_kd}\sigma_{x_2}\sigma_{y_2}}\right)\right]^j. \#(47)$$

### 3.2.1 OP for TSR protocol

The OP for multiple DF relays with BRS using WPT protocol TSR can be written as follows by substituting the values for $\alpha_{sr_k} = \frac{2\eta\alpha P_{PB}}{A_{sr_k}A_{PB_S}(1-\alpha)N_{sr_k}}$ and $\alpha_{r_kd} = \frac{2\eta\alpha P_{PB}}{A_{r_kd}A_{PB_{R_k}}(1-\alpha)N_{r_kd}}$ in (47).

$$P_{Out}(f,d) = 1 + \sum_{j=1}^{K} \binom{K}{j} (-1)^j \left[\frac{\gamma_{th}^2 A_{sr_k}A_{PB_S}A_{r_kd}A_{PB_{R_k}}(1-\alpha)^2 N_{sr_k}N_{r_kd}}{4\eta^2\alpha^2(P_{PB})^2\sigma_{x_1}\sigma_{y_1}\sigma_{x_2}\sigma_{y_2}}\right.$$
$$\left. \times K_1\left(\frac{\gamma_{th}A_{sr_k}A_{PB_S}(1-\alpha)N_{sr_k}}{2\eta\alpha P_{PB}\sigma_{x_1}\sigma_{y_1}}\right) K_1\left(\frac{\gamma_{th}A_{r_kd}A_{PB_{R_k}}(1-\alpha)N_{r_kd}}{2\eta\alpha P_{PB}\sigma_{x_2}\sigma_{y_2}}\right)\right]^j. \#(48)$$

### 3.2.2 OP for PSR Protocol

The OP for multiple DF relays with BRS using WPT protocol PSR can be written as follows by substituting the values for $\alpha_{sr_k} = \frac{\eta\rho(1-\rho)P_{PB}}{A_{sr_k}A_{PB_S}N_{sr_k}}$ and $\alpha_{r_kd} = \frac{\eta\rho(1-\rho)P_{PB}}{A_{r_kd}A_{PB_{R_k}}N_{r_kd}}$ in (47).

$$P_{Out}(f,d) = 1 + \sum_{j=1}^{K} \binom{K}{j} (-1)^j \left[\frac{\gamma_{th}^2 A_{sr_k}A_{PB_S}A_{r_kd}A_{PB_{R_k}}N_{sr_k}N_{r_kd}}{\eta^2\rho^2(1-\rho)^2(P_{PB})^2\sigma_{x_1}\sigma_{y_1}\sigma_{x_2}\sigma_{y_2}}\right.$$
$$\left. \times K_1\left(\frac{\gamma_{th}A_{sr_k}A_{PB_S}N_{sr_k}}{\eta\rho(1-\rho)P_{PB}\sigma_{x_1}\sigma_{y_1}}\right) K_1\left(\frac{\gamma_{th}A_{r_kd}A_{PB_{R_k}}N_{r_kd}}{\eta\rho(1-\rho)P_{PB}\sigma_{x_2}\sigma_{y_2}}\right)\right]^j. \#(49)$$

### 3.3 Multiple DF Relays with Multiple DF Hops using BRS

The OP for multiple DF relays with multiple DF hops using WPT as in **Fig. 5**, can be calculated as

$$F_{\gamma_d}(\gamma_{th}) = \prod_{k=1}^{K} F_{\gamma_k}(\gamma_{th}), \#(50)$$

where $F_{\gamma_k}(\gamma_{th})$ is the end-to-end CDF for the particular relay, which can be stated as

$$F_{\gamma_k}(\gamma_{th}) = \left[1 - \left(1 - F_{\gamma_{sr_{1,k}}}(\gamma_{th})\right)\prod_{n=1}^{N}\left(1 - F_{\gamma_{r_{n,k}d}}(\gamma_{th})\right)\right]. \#(51)$$

Since $\gamma_{sr_{1,k}}$ and $\gamma_{r_{n,k}d}$ are independent Rayleigh distributed random variables, the CDFs of $F_{sr_{1,k}}(\gamma_{th})$ and $F_{r_{n,k}d}(\gamma_{th})$ can be written as follows

$$F_{\gamma_{sr_{1,k}}}(\gamma_{th}) = \int_0^{\infty} F_{y_1}\left(\frac{\gamma_{th}}{\alpha_{sr_1}x_1}\right) f_{x_1}(x_1)dx_1, \#(52)$$

$$F_{\gamma_{r_{n,k}d}}(\gamma_{th}) = \int_0^{\infty} F_{y_2}\left(\frac{\gamma_{th}}{\alpha_{r_nd}x_2}\right) f_{x_2}(x_2)dx_2, \#(53)$$

where $y_1 = \left|h_{sr_{1,k}}\right|^2$, $y_2 = \left|h_{r_{n,k}d}\right|^2$, $x_1 = \left|g_{PB_s}\right|^2$, and $x_2 = \left|g_{PB_{R_{n,k}}}\right|^2$. After some mathematical manipulations (52) and (53) can be written as

$$F_{\gamma_{sr_{1,k}}}(\gamma_{th}) = \int_0^{\infty} \frac{x_1}{\sigma_{x_1}^2} e^{-x_1^2/2\sigma_{x_1}^2} dx_1 - \int_0^{\infty} \frac{x_1}{\sigma_{x_1}^2} e^{-x_1^2/2\sigma_{x_1}^2} e^{-\left(\frac{\gamma_{th}}{\alpha_{sr_1}x_1}\right)^2/2\sigma_{y_1}^2} dx_1, \#(54)$$

$$F_{\gamma_{r_{n,k}d}}(\gamma_{th}) = \int_0^{\infty} \frac{x_2}{\sigma_{x_2}^2} e^{-x_2^2/2\sigma_{x_2}^2} dx_2 - \int_0^{\infty} \frac{x_2}{\sigma_{x_2}^2} e^{-x_2^2/2\sigma_{x_2}^2} e^{-\left(\frac{\gamma_{th}}{\alpha_{r_nd}x_2}\right)^2/2\sigma_{y_2}^2} dx_2. \#(55)$$

(54) and (55) can be calculated using [ [34], page 337, Eq. 3.326, $2^{10}$] and [ [34], page 370, Eq. 3.478, 4], and can be written as

$$F_{\gamma_{sr_{1,k}}}(\gamma_{th}) = \Gamma(1) - \frac{\gamma_{th}}{\alpha_{sr_1}\sigma_{x_1}\sigma_{y_1}} K_1\left(\frac{\gamma_{th}}{\alpha_{sr_1}\sigma_{x_1}\sigma_{y_1}}\right), \#(56)$$

$$F_{\gamma_{r_{n,k}d}}(\gamma_{th}) = \Gamma(1) - \frac{\gamma_{th}}{\alpha_{r_nd}\sigma_{x_2}\sigma_{y_2}} K_1\left(\frac{\gamma_{th}}{\alpha_{r_nd}\sigma_{x_2}\sigma_{y_2}}\right). \#(57)$$

By substituting (56) and (57) in (51), $F_{\gamma_k}(\gamma_{th})$ can be written as

$$F_{\gamma_k}(\gamma_{th}) = \left[1 - \frac{\gamma_{th}}{\alpha_{sr_1}\sigma_{x_1}\sigma_{y_1}} K_1\left(\frac{\gamma_{th}}{\alpha_{sr_1}\sigma_{x_1}\sigma_{y_1}}\right)\prod_{n=1}^{N}\frac{\gamma_{th}}{\alpha_{r_nd}\sigma_{x_2}\sigma_{y_2}} K_1\left(\frac{\gamma_{th}}{\alpha_{r_nd}\sigma_{x_2}\sigma_{y_2}}\right)\right], \#(58)$$

and by substituting (58) in (50), $F_{\gamma_d}(\gamma_{th})$ can be stated as

$$F_{\gamma_d}(\gamma_{th}) = \prod_{k=1}^{K}\left[1 - \frac{\gamma_{th}}{\alpha_{sr_1}\sigma_{x_1}\sigma_{y_1}} K_1\left(\frac{\gamma_{th}}{\alpha_{sr_1}\sigma_{x_1}\sigma_{y_1}}\right)\prod_{n=1}^{N}\frac{\gamma_{th}}{\alpha_{r_nd}\sigma_{x_2}\sigma_{y_2}} K_1\left(\frac{\gamma_{th}}{\alpha_{r_nd}\sigma_{x_2}\sigma_{y_2}}\right)\right]. \#(59)$$

For i.i.d. Rayleigh fading channels, the above equation can be further simplified to

$$F_{\gamma_d}(\gamma_{th}) = \left[1 - \frac{\gamma_{th}}{\alpha_{sr_1}\sigma_{x_1}\sigma_{y_1}} K_1\left(\frac{\gamma_{th}}{\alpha_{sr_1}\sigma_{x_1}\sigma_{y_1}}\right)\prod_{n=1}^{N}\frac{\gamma_{th}}{\alpha_{r_nd}\sigma_{x_2}\sigma_{y_2}} K_1\left(\frac{\gamma_{th}}{\alpha_{r_nd}\sigma_{x_2}\sigma_{y_2}}\right)\right]^K. \#(60)$$

Applying the mathematical identity in (46) to (60), $F_{\gamma_d}(\gamma_{th})$ can be written as

$$F_{\gamma_d}(\gamma_{th}) = \sum_{j=0}^{K}\binom{K}{j}(-1)^j\left[\frac{\gamma_{th}}{\alpha_{sr_1}\sigma_{x_1}\sigma_{y_1}} K_1\left(\frac{\gamma_{th}}{\alpha_{sr_1}\sigma_{x_1}\sigma_{y_1}}\right)\prod_{n=1}^{N}\frac{\gamma_{th}}{\alpha_{r_nd}\sigma_{x_2}\sigma_{y_2}} K_1\left(\frac{\gamma_{th}}{\alpha_{r_nd}\sigma_{x_2}\sigma_{y_2}}\right)\right]^j. \#(61)$$

### 3.3.1 OP for TSR protocol

The OP for multiple DF relays with multiple DF hops with BRS using WPT protocol TSR can be written as follows by substituting the values for $\alpha_{sr_{1,k}} = \frac{2\eta\alpha P_{PB}}{A_{sr_{1,k}} A_{PB_S}(1-\alpha)N_{sr_{1,k}}}$ and $\alpha_{r_{n,k}d} = \frac{2\eta\alpha P_{PB}}{A_{r_{n,k}d} A_{PB_{R_{n,k}}}(1-\alpha)N_{r_{n,k}d}}$ in (61).

$$P_{Out}(f,d) = 1 + \sum_{j=1}^{K} \binom{K}{j} (-1)^j \left[ \frac{\gamma_{th} A_{sr_{1,k}} A_{PB_S} (1-\alpha) N_{sr_{1,k}}}{2\eta\alpha P_{PB} \sigma_{x_1} \sigma_{y_1}} \right., \#(62)$$
$$\times K_1 \left( \frac{\gamma_{th} A_{sr_{1,k}} A_{PB_S} (1-\alpha) N_{sr_{1,k}}}{2\eta\alpha P_{PB} \sigma_{x_1} \sigma_{y_1}} \right) \prod_{n=1}^{N} \frac{\gamma_{th} A_{r_{n,k}d} A_{PB_{R_{n,k}}} (1-\alpha) N_{r_{n,k}d}}{2\eta\alpha P_{PB} \sigma_{x_2} \sigma_{y_2}}$$
$$\left. \times K_1 \left( \frac{\gamma_{th} A_{r_{n,k}d} A_{PB_{R_{n,k}}} (1-\alpha) N_{r_{n,k}d}}{2\eta\alpha P_{PB} \sigma_{x_2} \sigma_{y_2}} \right) \right]^j .$$

### 3.3.2 OP for PSR Protocol

The OP for multiple DF relays with multiple DF hops with BRS using WPT protocol PSR can be written as follows by substituting the values for $\alpha_{sr_{1,k}} = \frac{\eta\rho(1-\rho)P_{PB}}{A_{sr_{1,k}} A_{PB_S} N_{sr_{1,k}}}$ and $\alpha_{r_{n,k}d} = \frac{\eta\rho(1-\rho)P_{PB}}{A_{r_{n,k}d} A_{PB_{R_{n,k}}} N_{r_{n,k}d}}$ in (61).

$$P_{Out}(f,d) = 1 + \sum_{j=1}^{K} \binom{K}{j} (-1)^j \left[ \frac{\gamma_{th} A_{sr_{1,k}} A_{PB_S} N_{sr_{1,k}}}{\eta\rho(1-\rho) P_{PB} \sigma_{x_1} \sigma_{y_1}} \right., \#(63)$$
$$\times K_1 \left( \frac{\gamma_{th} A_{sr_{1,k}} A_{PB_S} N_{sr_{1,k}}}{\eta\rho(1-\rho) P_{PB} \sigma_{x_1} \sigma_{y_1}} \right) \prod_{n=1}^{N} \frac{\gamma_{th} A_{r_{n,k}d} A_{PB_{R_{n,k}}} N_{r_{n,k}d}}{\eta\rho(1-\rho) P_{PB} \sigma_{x_2} \sigma_{y_2}}$$
$$\left. \times K_1 \left( \frac{\gamma_{th} A_{r_{n,k}d} A_{PB_{R_{n,k}}} N_{r_{n,k}d}}{\eta\rho(1-\rho) P_{PB} \sigma_{x_2} \sigma_{y_2}} \right) \right]^j .$$

## 4. Results and Discussion

A standard medium of 1 percent water vapor molecules has been considered for all scenarios. Furthermore, for the scenarios considered, the value of Rayleigh fading parameter is $\sigma_i = 5$ unless stated otherwise. The transmission windows have been chosen after taking into consideration the following papers [12], [37], [38], and [39]. According to [12], transmission windows with minimum attenuation are located at 300GHz, 350GHz, 410GHz, 670GHz, and 850GHz bands. Monte-Carlo simulations have verified all analytical results.

**Table 1.** Parameters and Constants of Molecular Absorptions

| Symbol | Quantity | Units |
|---|---|---|
| $h$ | Planck constant | $6.6262 \times 10^{-34}$Js |
| $k_B$ | Boltzmann constant | $1.3806 \times 10^{-23}$J/K |
| $c$ | Speed of light in the vacuum | $2.9979 \times 10^{8}$m/s |
| $R$ | Gas constant | $8.20575 \times 10^{-5}$m$^{-3}$atm/K/mol |
| $N_A$ | Avogadro constant | $6.0221 \times 10^{23}$molecule/mol |
| $p$ | System pressure | [atm] |
| $p_0$ | Reference pressure | 1 atm |
| $T$ | System temperature | [K] |
| $T_0$ | Reference temperature | 296.0K |
| $T_{STP}$ | Temperature at Standard Pressure | 273.15K |
| $q^{i,g}$ | Mixing ratio of isotopologue *i* of gas *g* | [%] |
| $Q^{i,g}$ | Number of molecules per volume unit of isotopologue *i* of gas *g* | [molecule / m$^3$] |
| $k^{i,g}$ | Absorption coefficient for isotopologue *i* of gas *g* | m$^{-1}$ |
| $\sigma^{i,g}$ | Absorption cross section of isotopologue *i* of gas *g* | [m$^2$ / molecule] |
| $S^{i,g}$ | Absorption peak amplitude of isotopologue *i* of gas *g* | [Hz m$^2$ / molecule] |
| $G^{i,g}$ | Spectral lines shape of isotopologue *i* of gas *g* | [Hz$^{-1}$] |
| $F^{i,g}$ | Van Vleck-Weisskopf line shape for isotopologue *i* of gas *g* | [Hz$^{-1}$] |
| $f_c^{i,g}$ | Resonant frequency of isotopologue *i* of gas *g* | [Hz] |
| $f_{c0}^{i,g}$ | Resonant frequency of isotopologue *i* of gas *g* at reference pressure $p_0$ | [Hz] |
| $\delta^{i,g}$ | Linear pressure shift of isotopologue *i* of gas *g* | [Hz] |
| $\alpha_L^{i,g}$ | Lorentz half-width for isotopologue *i* of gas *g* | [Hz] |
| $\alpha_0^{air}$ | Broadening coefficient of air | [Hz] |
| $\alpha_0^{i,g}$ | Broadening coefficient of isotopologue *i* of gas *g* | [Hz] |
| $\gamma$ | Temperature broadening coefficient | [NA] |

### 4.1 Single DF Relay

**Fig. 6** and **Fig. 7** are respectively OP vs $\rho$ and $\alpha$. From **Fig. 6**, it is evident that the best OP performances have been obtained at $\rho = 0.5$, and we can observe in **Fig. 7** that the OP performances have improved as the value of $\alpha$ has increased.

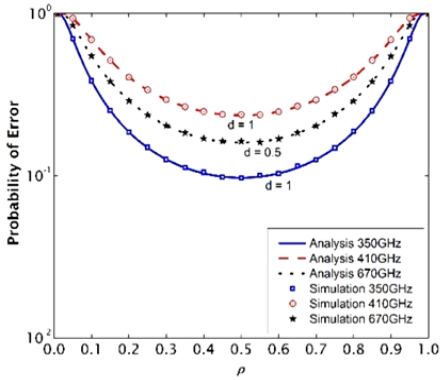


**Fig. 6.** OP vs $\rho$, 350GHz, 410GHz, 670GHz with PSR protocol, $P_{PB}$ = 1, $\eta$ = 1.

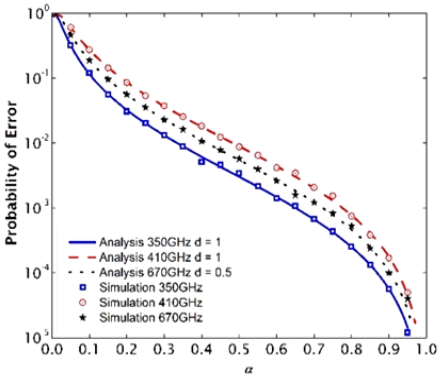


**Fig. 7.** OP vs $\alpha$, 350GHz, 410GHz, 670GHz with TSR protocol, $P_{PB}$ = 1, $\eta$ = 1.

**Fig. 8** and **Fig. 9** are respectively OP vs $\eta$ for PSR protocol and TSR protocol, and it is possbile to infer that OP performances improve as the value of $\eta$ is increased from 0 to 1.

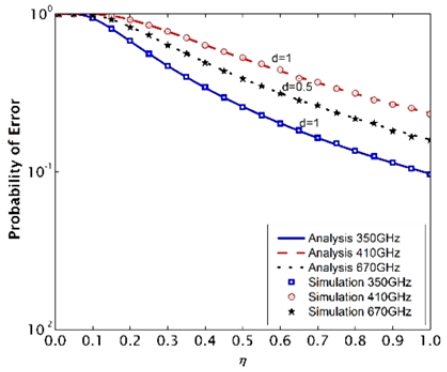


**Fig. 8.** OP vs $\eta$, 350GHz, 410GHz, 670GHz with PSR protocol, $P_{PB}$ = 1, $\rho$ = 0.5.

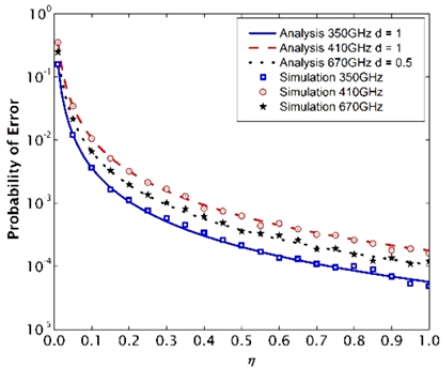


**Fig. 9.** OP vs $\eta$, 350GHz, 410GHz, 670GHz with TSR protocol, $P_{PB}$ = 1, $\alpha$ = 0.9.

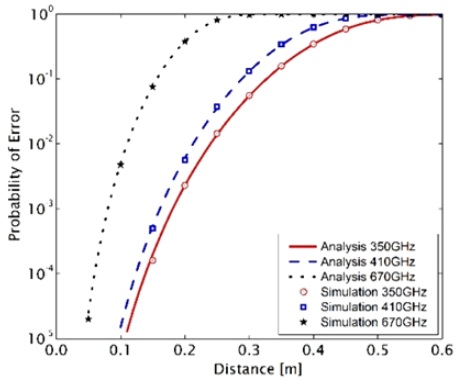


**Fig. 10.** OP vs Distance, 350GHz, 410GHz, 670GHz with PSR protocol, $P_{PB}$ = 10 * $10^{-3}$, $\eta$ = 0.8, $\rho$ = 0.5

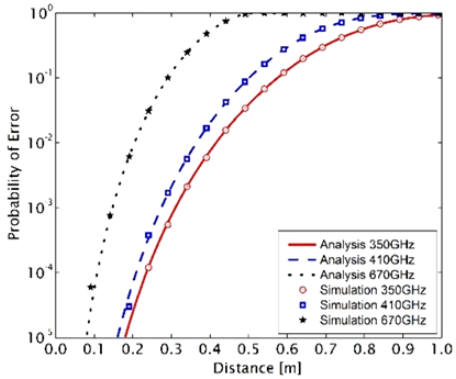


**Fig. 11.** OP vs Distance, 350GHz, 410GHz, 670GHz with TSR protocol, $P_{PB}$ = 10 * $10^{-3}$, $\eta$ = 0.8, $\rho$ = 0.6

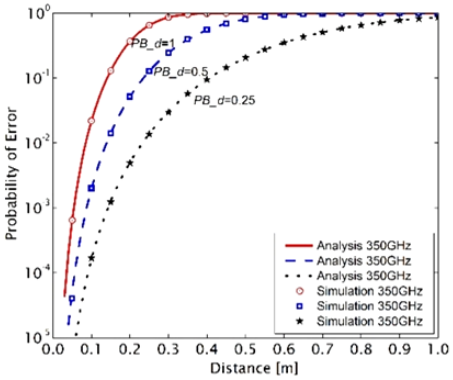


**Fig. 12.** OP vs Distance, 350GHz with PSR protocol, $P_{PB}$ = 10 * $10^{-3}$, $\eta$ = 0.8, $\rho$ = 0.5

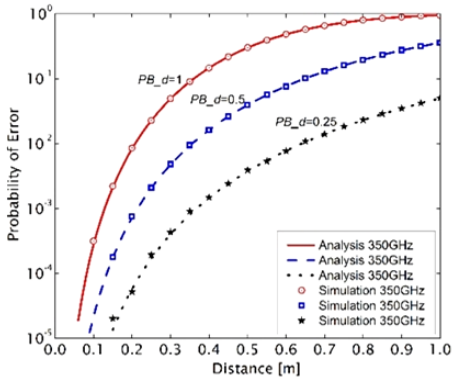


**Fig. 13.** OP vs Distance, 350GHz with TSR protocol, $P_{PB}$ = 10 * $10^{-3}$, $\eta$ = 0.8, $\rho$ = 0.6

From **Fig. 10** and **Fig. 11**, OP vs distance performances for single DF relay with WPT over 350GHz, 410GHz, and 670GHz bands have been compared respectively for PSR protocol and TSR protocol. It is possible to see that the best OP performances have been obtained in the 350GHz band for both PSR protocol and TSR protocol. Furthermore, from **Fig. 12** and **Fig. 13**, it is evident that the OP performances for PSR and TSR protocols for a single DF relay decrease as expected when the power beacon is further away from the nano machines.

### 4.2 Multiple DF Relays with BRS

OP for multiple DF relays using WPT over i.i.d. Rayleigh fading channels with BRS scheme have been analyzed for the scenarios of 2, 3, and 5 relays using WPT based on TSR protocol and PSR protocol, and are presented from **Fig. 14** to **Fig. 21**. It can be inferred from the above mentioned figures that by increasing the number of relays in a network, it is possible to obtain better OP performances. From **Fig. 20** and **Fig. 21**, it is evident that the best OP performances have been achieved for both PSR protocol and TSR protocol in the 350GHz transmission window. The best OP performances for PSR protocol have been obtained when $\rho = 0.5$. For TSR protocol, as the number of relays is increased, the required faction of time of $\alpha$ is decreased. Furthermore, it is evident from the following figures that as $\eta$ is increased, OP performances for PSR protocol and TSR protocol are improved.

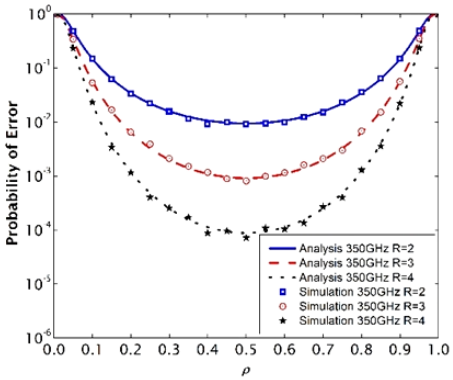


**Fig. 14.** OP vs $\rho$, over 350GHz with PSR protocol for Multiple DF Relays, $P_{PB}$ = 1, $\eta$ = 1, d = 1.

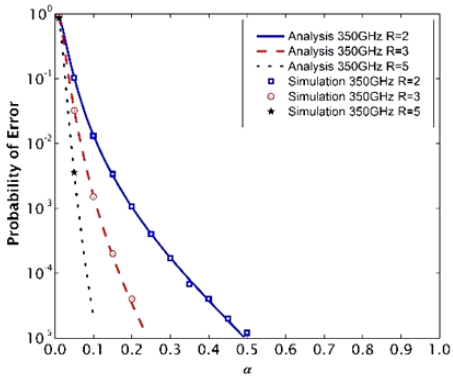


**Fig. 15.** OP vs $\alpha$, over 350GHz with TSR protocol for Multiple DF Relays, $P_{PB}$ = 1, $\eta$ = 1, d = 1.

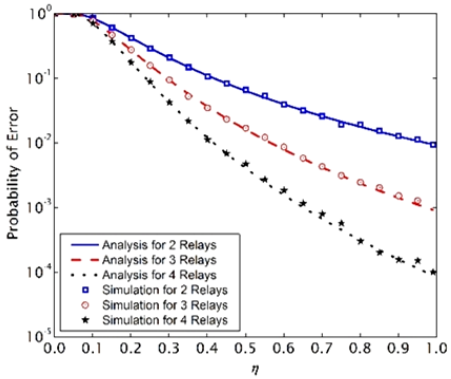


**Fig. 16.** OP vs $\eta$, over 350GHz with PSR protocol for Multiple DF Relays, $P_{PB}$ = 1, $\rho$ = 0.5, d = 1.

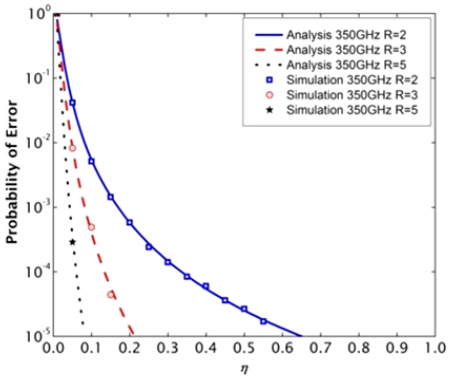


**Fig. 17.** OP vs $\eta$, over 350GHz with TSR protocol for Multiple DF Relays, $P_{PB}$ = 1, $\alpha$ = 0.6, d = 1.

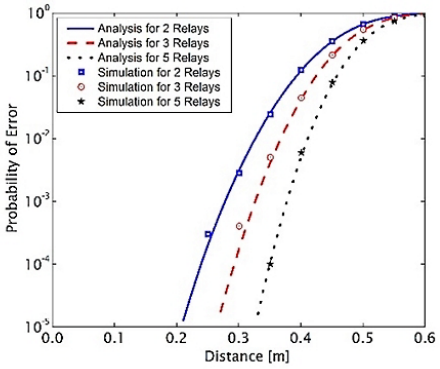


**Fig. 18.** OP vs Distance, 350GHz with PSR protocol for Multiple DF Relays, $P_{PB}$ = 10 * $10^{-3}$, $\eta$ = 0.8, $\rho$ = 0.5.

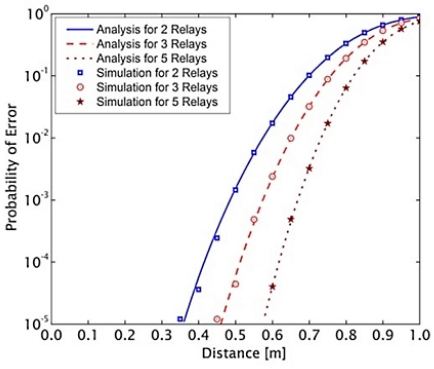


**Fig. 19.** OP vs Distance, 350GHz with TSR protocol for Multiple DF Relays, $P_{PB}$ = 10 * $10^{-3}$, $\eta$ = 0.8, $\alpha$ = 0.6.

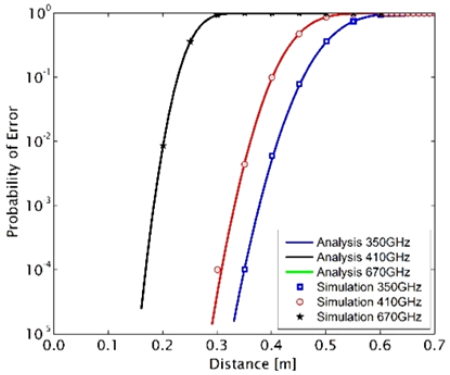


**Fig. 20.** OP vs Distance, 350GHz, 410GHz, 670GHz, with PSR protocol for Multiple DF Relays, Relays = 5, $P_{PB}$ = 10 * $10^{-3}$, $\eta$ = 0.8, $\rho$ = 0.5.

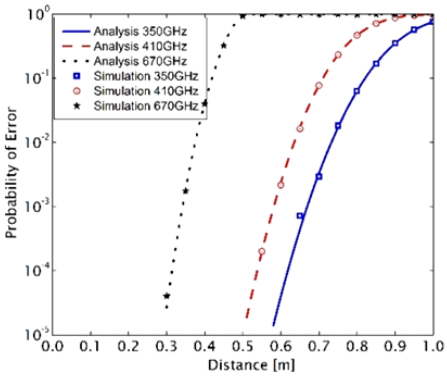


**Fig. 21.** OP vs Distance, 350GHz, 410GHz, 670GHz, with TSR protocol for Multiple DF Relays, Relays = 5, $P_{PB}$ = 10 * $10^{-3}$, $\eta$ = 0.8, $\alpha$ = 0.6.

### 4.3 Multiple DF Relays with Multiple DF Hops using BRS

OP for multiple DF relays with multiple DF hops per relay over i.i.d. Rayleigh fading channels with BRS scheme using WPT are investigated from **Fig. 22** to **Fig. 27**. In **Fig. 22** and **Fig. 23**, a single DF relay with multiple DF hops with WPT using PSR protocol and TSR protocol have been respectively investigated. It is possible to see from the graphs that by increasing the number of hops from 2 to 5, the OP performances have only been degraded minutely. In **Fig. 26**, multiple DF relays with multiple DF hops using PSR protocol, and in **Fig. 27**, multiple DF relays with multiple DF hops using TSR protocol have been investigated. For the scenarios considered in the graphs mentioned, there are 5 hops per relay. Futhermore, it can be observed from **Fig. 26** and **Fig. 27** that by increasing the number of relays from 1 to 5, the OP performances are increased significantly respectively for PSR protocol and TSR protocol. Moreover from **Fig. 24** and **Fig. 25**, it is possible to see that the best OP performances have been obtained in the 350GHz transmission window.

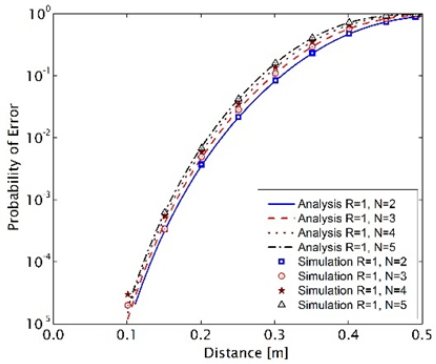


**Fig. 22.** OP vs Distance, 350GHz using PSR protocol for Single Relay With Multiple DF Hops, $P_{PB} = 10 * 10^{-3}$, $\rho = 0.5$, $\eta = 0.8$.

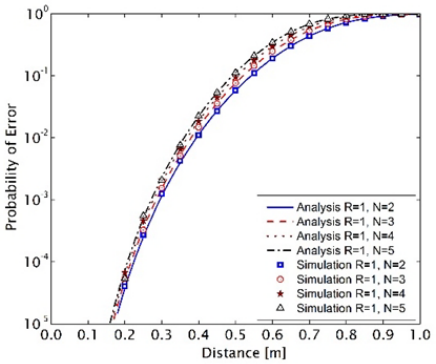


**Fig. 23.** OP vs Distance, 350GHz using TSR protocol for Single Relay With Multiple DF Hops, $P_{PB} = 10 * 10^{-3}$, $\alpha = 0.6$, $\eta = 0.8$.

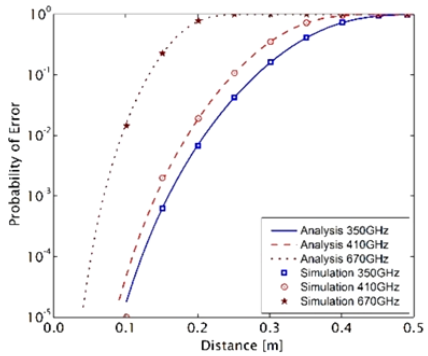


**Fig. 24.** OP vs Distance, 350GHz, 410GHz, 670GHz using PSR protocol for Single Relay With Multiple DF Hops, Hops = 5, $P_{PB} = 10 * 10^{-3}$, $\rho = 0.5$, $\eta = 0.8$.

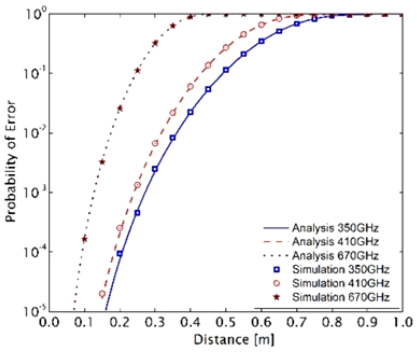


**Fig. 25.** OP vs Distance, 350GHz, 410GHz, 670GHz using TSR protocol for Single Relay With Multiple DF Hops, Hops = 5, $P_{PB} = 10 * 10^{-3}$, $\alpha = 0.6$, $\eta = 0.8$.

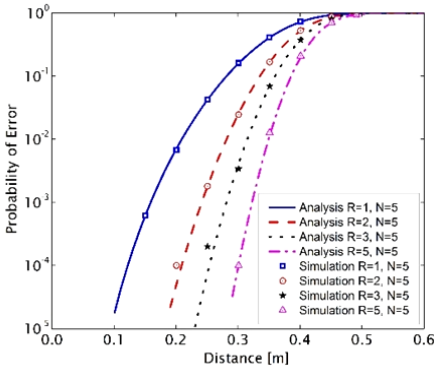


**Fig. 26.** OP vs Distance, 350GHz window using PSR protocol for Multiple Relay With Multiple Hops, $P_{PB} = 10 * 10^{-3}$, $\rho = 0.5$, $\eta = 0.8$.

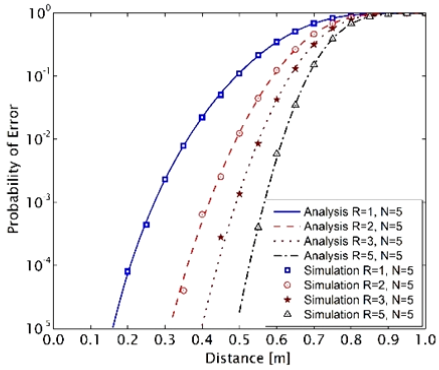


**Fig. 27.** OP vs Distance, 350GHz window using TSR protocol for Multiple Relays With Multiple Hops, $P_{PB} = 10 * 10^{-3}$, $\alpha = 0.6$, $\eta = 0.8$.

## 5. Conclusion

One of the major hurdles associated with nano communications is the limited amount of transmission power available for nano devices. In this paper, we have proposed using cooperative communication techniques with wireless power transfer protocols TSR and PSR to extend the transmission distances through relaying. Terahertz band is capable of very high capacity and very high transmission bit rates. Furthermore, the Terahertz band is rarely utilized currently. Therefore, cooperative communication among nano devices in the Terahertz band with wireless power transfer can provide significant improvements to the capabilities of nano-devices / machines.

The results have shown that by increasing the number of relays, it is possible to get better OP performance. In addition, it has shown that by increasing the number of hops per relay from 2 to 5, the OP performances were not affected significantly. Therefore, the range between the source nano machine and the destination nano machine can be significantly boosted through cooperative communication with wireless power transfer, which will enable nano technology in diverse fields ranging from national security application to health care monitoring systems. Furthermore, it is evident from the results that the best OP performances are observed in the 350GHz transmission window.

From the results obtained, it is possible to see that as the energy conversion efficiency increases from 0 to 1, the OP performances improve, and that the energy conversion efficiency required for same outage probability decreases as the number of relays increases. It is also possible to observe that as the transmission frequency increases, the required energy conversion efficiency increases to obtain the same outage probability.

For wireless power transfer using power switching relaying protocol, the best outage probability performances have been obtained when $\rho = 0.5$, and for wireless power transfer using time switching relay protocol, when the fraction of time used for energy harvesting (α) increases. Furthermore, the outage probability performances improve as the number of relays increases and the fraction of time needed for energy harvesting decreases. For time switching relaying protocol, as the fraction of time used for energy harvesting, α increases, the time available for information transmission decreases, and consequently the

throughput of the network decreases. Therefore, when deciding the value of α, throughput required for the cooperative nano communication network needs to be taken into consideration.

When the distance between the power beacon and the nano machines increases, the OP performances degrade.

Molecular absorption is dependent on frequency and distance. From the results obtained, it is possible to see that when the transmission frequency increases, the attenuation due to molecular absorption increases and the OP performances as well as the transmission distances decrease. Therefore, the relaying distances are dependent on the attenuation due to molecular absorption which is dependent on the frequency of operation and transmission energy. The amount of energy piezoelectric nano-generators are able to produce constantly is around 800pJ at the moment [15], [16], [17], and [18], therefore through wireless power transfer, it is possible to increase the power available for data transmission, etc. In the future, with further improvements in nanotechnology and THz band devices, the transmission distances could be further increased and better performances could be obtained. The analytical results have been verified by Monte-Carlo simulations for all the scenarios in this paper.

## References

[1] I. F. Akyildiz, F. Brunetti and C. BlÃ¡zquez, "Nanonetworks: A new communication paradigm," *Computer Networks*, vol. 52, no. 12, pp. 2260 - 2279, Aug. 2008. Article (CrossRef Link)

[2] I. F. Akyildiz and J. M. Jornet, "Electromagnetic wireless nanosensor networks," *Nano Communication Networks*, vol. 1, no. 1, pp. 3 - 19, March 2010. Article (CrossRef Link)

[3] J. M. Jornet and I. F. Akyildiz, "Channel Capacity of Electromagnetic Nanonetworks in the Terahertz Band," in *Proc. of Communications (ICC), 2010 IEEE International Conference on, Cape Town*, 2010. Article (CrossRef Link)

[4] Y. Okaie, T. Nakano, T. Hara and S. Nishio, "Distributing Nanomachines for Minimizing Mean Residence Time of Molecular Signals in Bionanosensor Networks," *IEEE Sensors Journal*, vol. 14, no. 1, pp. 218 - 227, Jan. 2014. Article (CrossRef Link)

[5] J. M. Jornet and I. F. Akyildiz, "Channel Modeling and Capacity Analysis for Electromagnetic Wireless Nanonetworks in the Terahertz Band," *IEEE Transactions on Wireless Communications*, vol. 10, no. 10, pp. 3211 - 3221, Oct. 2011. Article (CrossRef Link)

[6] compiled by the class for Physics of the Royal Swedish Academy of Sciences, "GRAPHENE, Scientific Background on the Nobel Prize in Physics 2010," *Physics of the Royal Swedish Academy of Sciences, Stockholm*, Oct. 2010. Article (CrossRef Link)

[7] P. Avouris, Z. Chen and V. Perebeiros, "Carbon-based electronics," *Nature Nanotechnology*, vol. 2, no. 10, pp. 605 - 615, Sep. 2007. Article (CrossRef Link)

[8] M. Dragoman, A. A. Muller, D. Dragoman, F. Coccetti and R. Plana, "Terahertz antenna based on graphene," *Journal of Applied Physics*, vol. 107, no. 10, May 2010. Article (CrossRef Link)

[9] J. M. Jornet and I. F. Akyildiz, "Graphene-based nano-antennas for electromagnetic nanocommunications in the terahertz band," in *Proc. of the Fourth European Conference on Antennas and Propagation, Barcelona*, 2010. Article (CrossRef Link)

[10] I. Llatser, C. Kremers, A. Cabellos-Aparicio, J. M. Jornet, E. AlarcÃ³n and D. N. Chigrin, "Graphene-based nano-patch antenna for terahertz radiation," *Photonics and Nanostructures - Fundamentals and Applications*, vol. 10, no. 4, pp. 353 - 358, May 2012. Article (CrossRef Link)

[11] J. C. Wiltse, "History of Millimeter and Submillimeter Waves," *IEEE Transactions on Microwave Theory and Techniques*, vol. 32, no. 9, pp. 1118 - 1127, Sep 1984. Article (CrossRef Link)

[12] T. Kleine-Ostmann and T. Nagatsuma, "A Review on Terahertz Communications Research," *Journal of Infrared, Millimeter, and Terahertz Waves*, vol. 32, no. 2, pp. 143 - 171, Feb. 2011. Article (CrossRef Link)

[13] J. Federici and L. Moeller, "Review of terahertz and subterahertz wireless communications," *Journal of Applied Physics*, vol. 107, no. 11, Jun 2010. Article (CrossRef Link)

[14] H. J. Song and T. Nagatsuma, "Present and Future of Terahertz Communications," *IEEE Transactions on Terahertz Science and Technology*, vol. 1, no. 1, pp. 256 - 263, Sep. 2011. Article (CrossRef Link)

[15] J. M. Jornet and I. F. Akyildiz, "Joint Energy Harvesting and Communication Analysis for Perpetual Wireless Nanosensor Networks in the Terahertz Band," *IEEE Transactions on Nanotechnology*, vol. 11, no. 3, pp. 570 - 580, May 2012. Article (CrossRef Link)

[16] Z. L. Wang, "Towards Self-Powered Nanosystems: From Nanogenerators to Nanopiezotronics," *Advanced Functional Materials*, vol. 18, no. 22, pp. 3553 - 3567, Nov. 2008. Article (CrossRef Link)

[17] S. Xu, B. J. Hansen and Z. L. Wang, "Piezoelectric-nanowire-enabled power source for driving wireless microelectronics," *Nature Communication*, vol. 1, no. 93, pp. 1 - 5, Oct. 2010. Article (CrossRef Link)

.[18] S. Xu, Y. Qin, C. Xu, Y. Wei, R. Yang and Z. L. Wang, "Self-powered nanowire devices," *Nature nanotechnology*, vol. 5, no. 5, pp. 366 - 373, May 2010. Article (CrossRef Link)

[19] C. R. Valenta and G. D. Durgin, "Harvesting Wireless Power: Survey of Energy-Harvester Conversion Efficiency in Far-Field, Wireless Power Transfer Systems," *IEEE Microwave Magazine*, vol. 154, no. 4, pp. 108-120, 2014. Article (CrossRef Link)

[20] N. Tesla, "Transmission of electrical energy without wires as a means for furthering peace," *Elect. World Eng.*,, pp. 21-24, Jan. 1905. Article (CrossRef Link)

[21] W. C. Brown, "The History of Power Transmission of Power Transmission by Radio Waves," *IEEE Transactions on Microwave Theory and Techniques*, vol. 32, no. 9, pp. 1230-1242, 1984. Article (CrossRef Link)

[22] R. Want, "An introduction to RFID technology," *IEEE Pervasive Computing*, vol. 5, no. 1, pp. 25-33, 2006. Article (CrossRef Link)

[23] A. Kurs, A. Karalis, R. Moffatt, J. D. Joannopoulos, P. Fisher and M. Solja, "Wireless Power Transfer via Strongly Coupled Magnetic Resonances," *American Association for Advancement of Science*, vol. 317, no. 5834, pp. 83-86, 2007. Article (CrossRef Link)

[24] K. Huang and V. N. Lau, "Enabling Wireless Power Transfer in Cellular Networks: Architecture, Modeling and Deployment," *IEEE Transactions on Wireless Communications*, vol. 13, no. 2, pp. 902-912, 2014. Article (CrossRef Link)

[25] L. R. Varshney, "Transporting information and energy simultaneously," in *Proc. of 2008 IEEE International Symposium on Information Theory*, pp. 1612-1616, 2008. Article (CrossRef Link)

[26] X. Zhou, R. Zhang and C. K. Ho, "Wireless Information and Power Transfer: Architecture Design and Rate-Energy Tradeoff," *IEEE Transactions on Communications*, vol. 61, no. 11, pp. 4754-4767, 2013. Article (CrossRef Link)

[27] R. Zhang and C. K. Ho, "MIMO Broadcasting for Simultaneous Wireless Information and Power Transfer," *IEEE Transactions on Wireless Communications*, vol. 12, no. 5, pp. 1989-2001, 2013. Article (CrossRef Link)

[28] H. Gao, W. Ejaz and M. Jo, "Cooperative Wireless Energy Harvesting and Spectrum Sharing in 5G Networks," *IEEE Access*, vol. 4, pp. 3647 - 3658, 2016. Article (CrossRef Link)

[29] S. A. Clough, F. X. Kneizys and R. W. Davies, "Line shape and the water vapor continuum," *Atmospheric Research*, vol. 23, no. 3, pp. 229 - 241, Jun. 1989. Article (CrossRef Link)

[30] J. H. Van Vleck and V. F. Weisskopf, "On the Shape of Collision-Broadened Lines," *Rev. Mod. Phys.*, vol. 17, no. 2 - 3, pp. 227 - 236, Apr 1945. Article (CrossRef Link)

[31] Y. Liu, L. Wang, M. Elkashlan, T. Q. Duong and A. Nallanathan, "Two-way relay networks with wireless power transfer: design and performance analysis," *IET Communications*, vol. 10, no. 14, pp. 1810-1819, 2016. Article (CrossRef Link)

[32] A. A. Nasir, X. Zhou, S. Durrani and R. A. Kennedy, "Relaying Protocols for Wireless Energy Harvesting and Information Processing," *IEEE Transactions on Wireless Communications*, vol. 12, no. 7, pp. 3622-3636, 2013. Article (CrossRef Link)

[33] X. Zhou, R. Zhang and C. K. Ho, "Wireless information and power transfer: Architecture design and rate-energy tradeoff," in *Proc. of 2012 IEEE Global Communication Conference*, 2012. Article (CrossRef Link)

[34] I. S. Gradshteyn and I. M. Ryzhik, *Table of Integrals, Series, and Products*, Elsevier Inc., London, 2007.

[35] V. N. Q. Bao, T. Doung, D. B. da Costa, G. Alexandropoulos and A. Nallanathan, "Cognitive amplify-and-forward relaying with best relay selection in non-identical rayleigh fading," *IEEE Commun. Lett.*, vol. 17, no. 3, pp. 475-478, 2013. Article (CrossRef Link)

[36] T. Doung, V. Bao, G. Alexandropoulos and H.-J. Zepernick, "Cooperative spectrum sharing networks with AF relay and selection diversity," *Electronic Letter*, vol. 47, no. 20, pp. 1149-1151, 2011. Article (CrossRef Link)

[37] R. Piesiewicz, T. Kleine-Ostmann, N. Krumbholz, D. Mittleman, M. Koch, J. Schoebei and T. Kurner, "Short-Range Ultra-Broadband Terahertz Communications: Concepts and Perspectives," *IEEE Antennas and Propagation Magazine*, vol. 49, no. 6, pp. 24 - 39, Dec 2007. Article (CrossRef Link)

[38] P. Boronin, V. Petrov, D. Moltchanov, Y. Koucheryavu and J. M. Jornet, "Capacity and throughput analysis of nanoscale machine communication through transparency windows in the terahertz band," *Nano Communication Networks*, vol. 5, no. 3, pp. 72-82, 2014. Article (CrossRef Link)

[39] R. Piesiewicz, J. Jemai, M. Koch and T. Kurner, "THz channel characterization for future wireless gigabit indoor communication systems," *SPIE*, vol. 5727, pp. 166-176, 2005. Article (CrossRef Link)

**A. Chaminda J. Samarasekera:** received a B.Sc degree in Avionics Engineering Technology from Embry-Riddle Aeronautical Engineering (Daytona Beach, Florida, USA) in 2004, and a M.Sc. degree in Electrical Engineering in the area of Radio Communication from Blekinge Institute of Technology (Karlskrona, Sweden) in 2014. He was a graduate researcher at the CCTLab in the Electronic Engineering department at Kyung Hee University (Yongin-si, Republic of Korea), till 2018. In 2018, he joined the institue of communications engineering and RF-Systems at Johannes Kepler University in Linz, Austria. His current research interest include wireless communication, Terahertz communication, Nano Communications, Wireless power transfer, Cognitive Radio, Cooperative Communications and RADAR systems.

**Hyundong Shin:** (S'01-M'04-SM'11) received the B.S. degree in electronics engineering from Kyung Hee University (KHU), Yongin-si, Korea, in 1999, and the M.S. and Ph.D. degrees in electrical engineering from Seoul National University, Seoul, Korea, in 2001 and 2004, respectively. During his postdoctoral research at the Massachusetts Institute of Technology (MIT) from 2004 to 2006, he was with the Wireless Communication and Network Sciences Laboratory within the Laboratory for Information Decision Systems (LIDS). In 2006, Dr. Shin joined the KHU, where he is now a Professor at the Department of Electronic Engineering. His research interests include quantum information science, wireless communication, and nanonetworks. Dr. Shin was honored with the Knowledge Creation Award in the field of Computer Science from Korean Ministry of Education, Science and Technology (2010). He received the IEEE Communications Society's Guglielmo Marconi Prize Paper Award (2008) and William R. Bennett Prize Paper Award (2012). He served as a Publicity co-chair for the IEEE PIMRC (2018) and a Technical Program co-chair for the IEEE WCNC (PHY Track 2009) and the IEEE Globecom (Communication Theory Symposium 2012, Cognitive Radio and Networks Symposium 2016). He was an Editor for IEEE Transactions on Wireless Communications (2007-2012) and IEEE Communications Letters (2013-2015).